Propiedades estructurales, ópticas y eléctricas de películas delgadas de ZnO obtenidas por oxidación térmica de Zn depositado por RF sputtering

Mahmoud Nabil*, Aurora Matias, Miguel Rivera, Pablo Amieva, Milenis Acosta

Facultad de Ingeniería, Universidad Autónoma de Yucatán, Industrias No Contaminantes S/N, 97302 Mérida, Yuc., Mexico

Fecha de recepción: 6 de marzo de 2026 - Fecha de aceptación: 6 de mayo de 2026

Resumen

En este trabajo se obtuvieron películas delgadas de óxido de zinc a partir de capas metálicas de zinc depositadas sobre sustratos de vidrio mediante sputtering por radiofrecuencia en condiciones no reactivas. Posteriormente, se investigaron sus propiedades estructurales, ópticas y eléctricas. Después del depósito de las capas de zinc, las películas fueron sometidas a tratamientos térmicos entre 300 y 600 °C con el objetivo de promover la formación del óxido. La caracterización estructural mediante difracción de rayos X confirmó la formación de ZnO policristalino con estructura hexagonal tipo wurtzita después del tratamiento térmico. La microscopía electrónica de barrido reveló películas porosas nanoestructuradas. Las mediciones ópticas mostraron que las muestras tratadas a 500 y 600 °C presentan alta transparencia en la región visible, con valores de transmitancia cercanos al 90%. A partir del análisis de Tauc se estimaron valores de energía de banda prohibida de aproximadamente 3.22 y 3.25 eV. La caracterización eléctrica mediante mediciones de efecto Hall reveló una transición de comportamiento metálico a semiconductor al aumentar la temperatura de tratamiento térmico, con valores de resistividad del orden de 10^{-2}–10^{-1} Ω·cm para las películas de ZnO. La película tratada a 500 °C presentó la mayor movilidad de portadores, con un valor aproximado de 13.5 $cm^2 \cdot V^{-1} \cdot s^{-1}$. Estos resultados demuestran que la oxidación térmica de películas de Zn depositadas por sputtering constituye una ruta simple y económica para producir películas delgadas nanoestructuradas de ZnO con propiedades adecuadas para aplicaciones optoelectrónicas.

Palabras clave: óxido de zinc; películas delgadas; sputtering por radiofrecuencia; propiedades optoelectrónicas; óxidos semiconductores

*t.mahmoud.nabil@correo.uady.mx

Nota: Este artículo de investigación es parte de Ingeniería–Revista Académica de la Facultad de Ingeniería, Universidad Autónoma de Yucatán, Vol. 30, No. 1, 2026, ISSN: 2448-8364

Properties of ZnO Thin Films: Structural, Optical, and Electrical Characteristics Derived from Thermal Oxidation of RF-Sputtered Zinc

Abstract

In this work, zinc oxide thin films were obtained from metallic zinc layers deposited on glass substrates by non-reactive radio-frequency magnetron sputtering, and their structural, optical, and electrical properties were investigated. After deposition, the films were thermally annealed at temperatures between 300 and 600 °C in order to promote the oxidation of Zn and the formation of ZnO. Structural characterization by X-ray diffraction confirmed the formation of polycrystalline ZnO with a hexagonal wurtzite structure after thermal treatment. Scanning electron microscopy revealed nanostructured porous films with grain sizes in the nanometer range. Optical measurements showed that samples annealed at 500 and 600 °C exhibit high transparency in the visible region, with transmittance values close to 90%. Optical band gap values of approximately 3.22 and 3.25 eV were estimated from Tauc analysis. Electrical characterization using Hall measurements revealed a transition from metallic to semiconducting behavior with increasing annealing temperature, with resistivity values on the order of 10^{-2}–10^{-1} Ω·cm for the ZnO films. The film annealed at 500 °C exhibited the highest carrier mobility of approximately 13.5 $cm^2 \cdot V^{-1} \cdot s^{-1}$. These results demonstrate that thermal oxidation of sputtered Zn films provides a simple and cost-effective route for producing nanostructured ZnO thin films with properties suitable for optoelectronic applications.

Keywords: Zinc oxide; thin films; radio-frequency sputtering; optoelectronic properties; semiconductor oxides.

Introduction

Zinc oxide (ZnO) is a II–VI semiconductor that has garnered significant attention due to its direct band gap of approximately 3.37 eV at room temperature and its large exciton binding energy of about 60 meV (Özgür et al., 2005; Raoufi, 2013). These properties enable efficient excitonic emission even at room temperature, making ZnO particularly appealing for optoelectronic applications, including flat panel displays, transparent electronics, and thin-film photovoltaic systems (Özgür et al., 2005; Raha & Ahmaruzzaman, 2022). Additionally, ZnO is known for its high chemical and mechanical stability, environmental friendliness, and natural abundance.

With the rapid advancement of nanotechnology, research has increasingly focused on understanding and controlling the properties of ZnO in nanostructured forms, particularly as thin films (Özgür et al., 2005; Kołodziejczak-Radzimska & Jesionowski, 2014; Janotti & Van de Walle, 2009). ZnO thin films are of particular interest for optoelectronic and photovoltaic applications due to their favorable electronic transport properties, optical transparency in the visible region, and compatibility with low-temperature fabrication processes. Specifically, ZnO has been extensively studied as both a transparent conductive oxide and an electron transport layer in various devices, owing to its relatively high electron mobility and favorable energy band alignment (Ellmer, 2012; Fortunato et al., 2012; Özgür et al., 2020). As a result, nanostructured ZnO thin films have been incorporated into several types of photovoltaic devices, including organic solar cells (White et al., 2006), dye-sensitized solar cells (O'Regan & Grätzel, 1991; Law et al.,

2005), and perovskite solar cells (Yang et al., 2016; Correa-Baena et al., 2017). The nanostructured morphology of ZnO offers large interfacial surface areas and efficient charge transport pathways, which are beneficial for these device architectures.

The structural, optical, and electrical properties of ZnO thin films are significantly influenced by the synthesis route and post-deposition treatments, which affect parameters such as crystallinity, morphology, and electronic transport characteristics (Janotti & Van de Walle, 2009; Kołodziejczak-Radzimska & Jesionowski, 2014). Various techniques have been developed to deposit ZnO thin films, including chemical vapor deposition, sol–gel processing, pulsed laser deposition, and sputtering methods (Özgür et al., 2005; Ellmer, 2012). Among these, magnetron sputtering is particularly appealing because it enables precise control of film thickness, good uniformity, high reproducibility, and compatibility with large-area deposition and industrial-scale production (Minami, 2005; Ellmer, 2001; Ellmer, 2012). Several studies have shown that radio-frequency (RF) magnetron sputtering can produce ZnO thin films with tunable structural and optoelectronic properties, depending on the deposition parameters and post-deposition treatments (Jeong et al., 2003; Ellmer, 2001). However, obtaining nanostructured ZnO films with desirable optical and electrical properties using physical vapor deposition techniques can still be challenging. In particular, reactive magnetron sputtering, in which oxygen is introduced directly into the deposition chamber, is susceptible to target poisoning, which leads to reduced deposition rates, process instability, and difficulties in achieving reproducible film properties (Ellmer, 2001; Minami, 2005). Alternatively, post-deposition thermal treatments can be employed to oxidize metallic Zn precursor films; while this approach simplifies the deposition step by eliminating reactive gases, it introduces additional processing steps and requires controlled thermal conditions.

Although thermal oxidation of sputtered metallic Zn as a route to ZnO thin films has been previously explored, a comprehensive evaluation of this approach for optoelectronic applications remains limited. Li et al. demonstrated that Zn films deposited by magnetron sputtering under non-reactive conditions (pure Ar) and subsequently oxidized at 600 °C yield dense ZnO layers with surface whiskers and low visible-range optical transmittance; high transparency was only achieved when oxygen was introduced into the sputtering gas, which causes partial oxidation of the target during deposition and complicates process control (Li et al., 2005). More recently, Hoffmann et al. employed controlled oxidation of sputtered Zn films at temperatures between 250 and 450 °C, focusing on defect microstructure characterization and thin-film transistor performance, with reported carrier mobilities of only 0.2 $cm^2/V \cdot s$ and without a systematic optical evaluation targeting optoelectronic applications (Hoffmann et al., 2021). Studies using thermal evaporation instead of sputtering as the Zn deposition method have addressed structural and optical properties but do not include electrical transport characterization (Sánchez-Dena et al., 2022), while high-power impulse magnetron sputtering-based approaches have been directed toward photocatalytic and antimicrobial applications rather than optoelectronic ones (Widyastuti et al., 2022). In this context, the present work provides a systematic and comprehensive characterization of the structural, morphological, optical, and electrical properties of ZnO thin films obtained by non-reactive RF magnetron sputtering of metallic Zn followed by post-deposition thermal annealing across a broad temperature range (300–600 °C). This approach eliminates the need for reactive sputtering during deposition, preventing target poisoning and simplifying process control. The results demonstrate that annealing temperature alone can be used to tune the properties of the resulting ZnO films, yielding nanostructured porous layers with optical transmittance

close to 90% in the visible region and carrier mobilities up to 13.5 $cm^2/V \cdot s$, through a simple and cost-effective fabrication route suitable for optoelectronic applications.

Experimental Methods

In RF magnetron sputtering, plasma ions bombard a target material, ejecting atoms that condense onto a substrate to form a thin film; when carried out in a purely inert atmosphere without reactive gases, the deposited film retains the composition of the target. Metallic Zn thin films were deposited on Corning 2947 glass substrates by non-reactive RF magnetron sputtering at room temperature. Depositions were carried out using an Intercovamex-V3 sputtering system equipped with a Lesker Torus magnetron gun connected to a 300 W Dressler Cesar RF power supply. A high-purity Zn target (Kurt J. Lesker, 99.99%) was used as the sputtering source, and the RF power during deposition was maintained at 100 W. The distance between the target and the substrate was fixed at 5.0 cm, and the deposition time was 10 minutes for all samples.

The glass substrates were cleaned ultrasonically in distilled water, acetone, and isopropyl alcohol (15 minutes each) before being introduced into the deposition chamber, in order to remove surface impurities. Before deposition, the vacuum chamber was evacuated using a turbomolecular pump, achieving a base pressure of approximately 2 x 10^{-5} Torr. Next, high-purity argon gas (99.999%) was introduced into the chamber, and the working pressure during sputtering was maintained at 5 mTorr. Before deposition, a pre-sputtering step of 3 minutes was performed under the same working conditions to remove any potential contaminants from the target surface. After deposition, the as-grown metallic zinc films were annealed at 300, 400, 500, and 600 °C for 2 hours under atmospheric conditions, enabling oxygen from the surrounding atmosphere to diffuse into the metallic Zn layer and react with Zn atoms to progressively form ZnO.

Film thickness was determined using a TRIBOtechnic stylus profilometer. Structural characterization was performed by X-ray diffraction (XRD) employing a Siemens D500 diffractometer with Cu Kα radiation (λ = 0.154 nm). The XRD measurements were conducted in grazing-incidence configuration at a fixed incidence angle of 1°, using a step size of 0.02° and a counting time of 3 s per step. Surface morphology and elemental composition were analyzed by field-emission scanning electron microscopy (FE-SEM) using a JEOL 7600F microscope equipped with an energy-dispersive X-ray spectroscopy (EDS) detector. Optical transmittance measurements were carried out using an Agilent 8453 UV–Vis spectrophotometer (ChemStation software) without an integrating sphere, over the wavelength range of 300–1100 nm with a spectral bandwidth of 1 nm. Electrical properties were evaluated at room temperature by Hall effect measurements using an Ecopia HMS-5000 system, employing the Van der Pauw contact geometry with silver ohmic contacts placed at the four corners of the sample and a magnetic flux density of 0.55 T.

Results and Discussion

Figure 1 shows the XRD patterns of the Zn thin films after annealing at temperatures ranging from 300 °C to 600 °C together with the as-deposited sample. The diffraction peaks observed in the annealed samples can be indexed to the hexagonal wurtzite structure of ZnO (JCPDS card No. 36-1451), indicating that the metallic Zn films were successfully converted into crystalline ZnO after thermal treatment. The most intense reflections appear at approximately 2θ = 31.7°, 34.4°, and 36.2°, corresponding to the (100), (002), and (101) crystallographic planes of ZnO, respectively. These reflections are characteristic of the hexagonal wurtzite structure and are consistent with standard diffraction data reported for ZnO

(Özgür et al., 2005; Janotti & Van de Walle, 2009).

Additional reflections corresponding to the (102), (110), (103), and (112) crystallographic planes of the hexagonal wurtzite structure can also be observed at approximately 2θ = 47.5°, 56.6°, 62.9°, and 67.9°, respectively, further confirming the formation of polycrystalline ZnO thin films (JCPDS card No. 36-1451). Similar diffraction patterns have been widely reported for ZnO materials exhibiting the wurtzite crystal structure, where the (100), (002), and (101) planes represent the most intense reflections in the XRD spectrum (Kołodziejczak-Radzimska & Jesionowski, 2014). The same characteristic diffraction peaks have also been observed in previous studies of ZnO nanostructures (Nabil et al., 2021), confirming the formation of pure hexagonal ZnO without secondary phases.

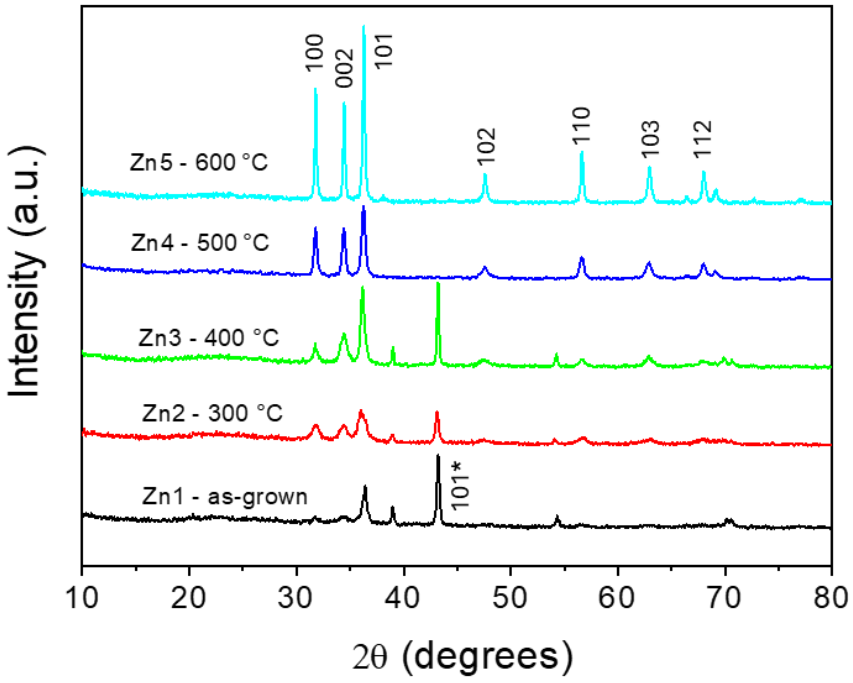

Figure 1. XRD patterns of the as-grown Zn thin film (Zn1) and ZnO thin films obtained by thermal annealing at 300 °C (Zn2), 400 °C (Zn3), 500 °C (Zn4), and 600 °C (Zn5). Miller indices indicate diffraction peaks corresponding to the hexagonal wurtzite structure of ZnO (JCPDS card No. 36-1451). The peak marked with an asterisk (*) at approximately 2θ ≈ 43° corresponds to the (101) reflection of residual metallic Zn in its hexagonal close-packed structure (JCPDS card No. 00-004-0831).

The as-deposited sample exhibits weak and relatively broad diffraction features, suggesting a low degree of crystallinity and the predominance of metallic Zn or poorly ordered structures. Notably, a weak diffraction peak at approximately 2θ ≈ 43° is observed in the patterns of the as-deposited sample and the films annealed at 300 °C and 400 °C, which can be attributed to the (101) reflection of residual metallic Zn in its hexagonal close-packed structure (JCPDS card No. 00-004-0831); this peak disappears at annealing temperatures of 500 °C and above, indicating that complete thermal oxidation of metallic Zn is achieved at these temperatures. After annealing at 300 °C, the emergence of ZnO diffraction peaks indicates the onset of oxidation and

crystallization of the sputtered Zn layer. As the annealing temperature increases to 400 °C and above, the diffraction peaks become sharper and more intense, revealing a progressive improvement in crystallinity and grain growth within the films. The reduction in peak broadening also suggests an increase in crystallite size and a decrease in structural defects such as lattice strain and dislocations as the annealing temperature increases, which is consistent with the enhanced structural ordering typically observed in thermally treated ZnO films.

The relative intensities of the diffraction peaks indicate that the films exhibit a polycrystalline structure without a strong preferential orientation, although the (101) reflection becomes particularly pronounced at higher annealing temperatures. Such variations in preferred orientation are commonly reported for ZnO thin films and are often associated with deposition parameters and thermal treatment conditions (Özgür et al., 2005). Overall, the XRD results demonstrate that annealing temperature strongly influences the oxidation of metallic Zn and the structural quality of the resulting ZnO thin films.

SEM was used to investigate the surface morphology of the deposited films and to evaluate the influence of the annealing temperature on the microstructure of the ZnO layers. The SEM images of the as-grown Zn thin film and the sample annealed at 300 °C are shown in Figure 2. Both samples exhibit very similar morphological characteristics. The films are composed of nanostructured grains forming a porous layer uniformly distributed across the substrate surface. At higher magnification, the particles display a nano-hexagonal morphology, which is consistent with the hexagonal wurtzite crystal structure identified by XRD analysis. Random particle size measurements performed from the SEM micrographs indicate grain sizes ranging from approximately 14 nm to 39 nm.

A noticeable change in morphology is observed for the films annealed at 400 °C, as shown in Figure 3. In this case, the surface is composed of larger agglomerated nanostructures forming irregular clusters distributed over the porous film. These structures appear as nonlinear aggregates composed of interconnected grains. Particle size measurements obtained from the SEM images indicate grain sizes ranging from approximately 43 nm to 74 nm, suggesting that thermal treatment promotes grain growth and structural rearrangement within the films.

The ZnO thin films annealed at 500 °C and 600 °C exhibit similar morphological characteristics, as shown in Figure 4. In both cases, the films are composed of uniformly distributed nanoparticles forming porous nanostructured layers. Compared with the as-grown sample, the grains appear more defined and slightly larger, indicating that higher annealing temperatures promote further crystallization and particle growth. Random particle size measurements show grain sizes ranging from approximately 22 nm to 69 nm. These results are consistent with the improvement in crystallinity observed in the XRD analysis, where higher annealing temperatures resulted in sharper diffraction peaks and reduced peak broadening.

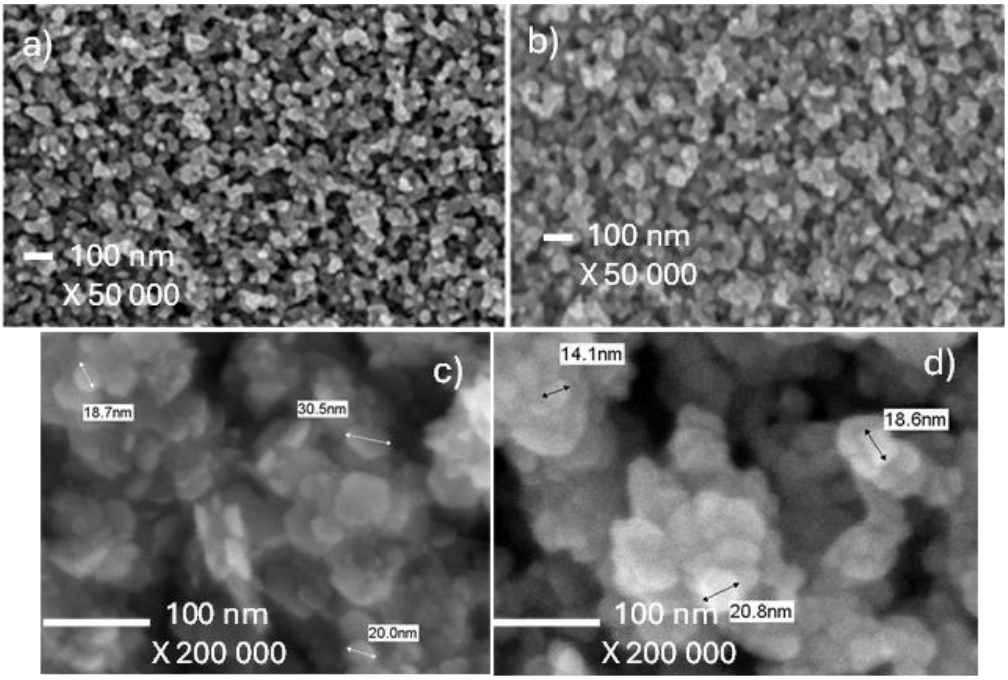

Figure 2. SEM images of Zn thin films: (a,c) as-grown sample at 50,000X and 200,000X magnification, respectively; (b,d) sample annealed at 300 °C at 50,000X and 200,000X magnification.

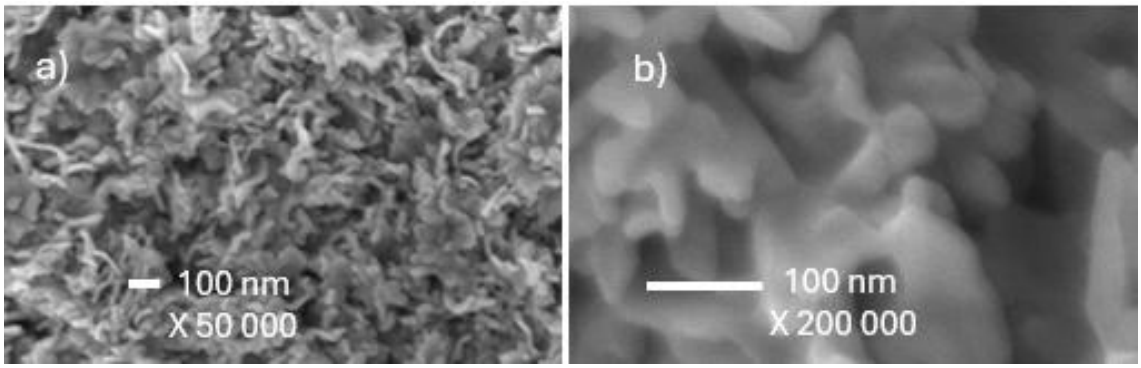

Figure 3. SEM images of ZnO thin films annealed at 400 °C, (a) 50,000X and (b) 200,000X magnification.

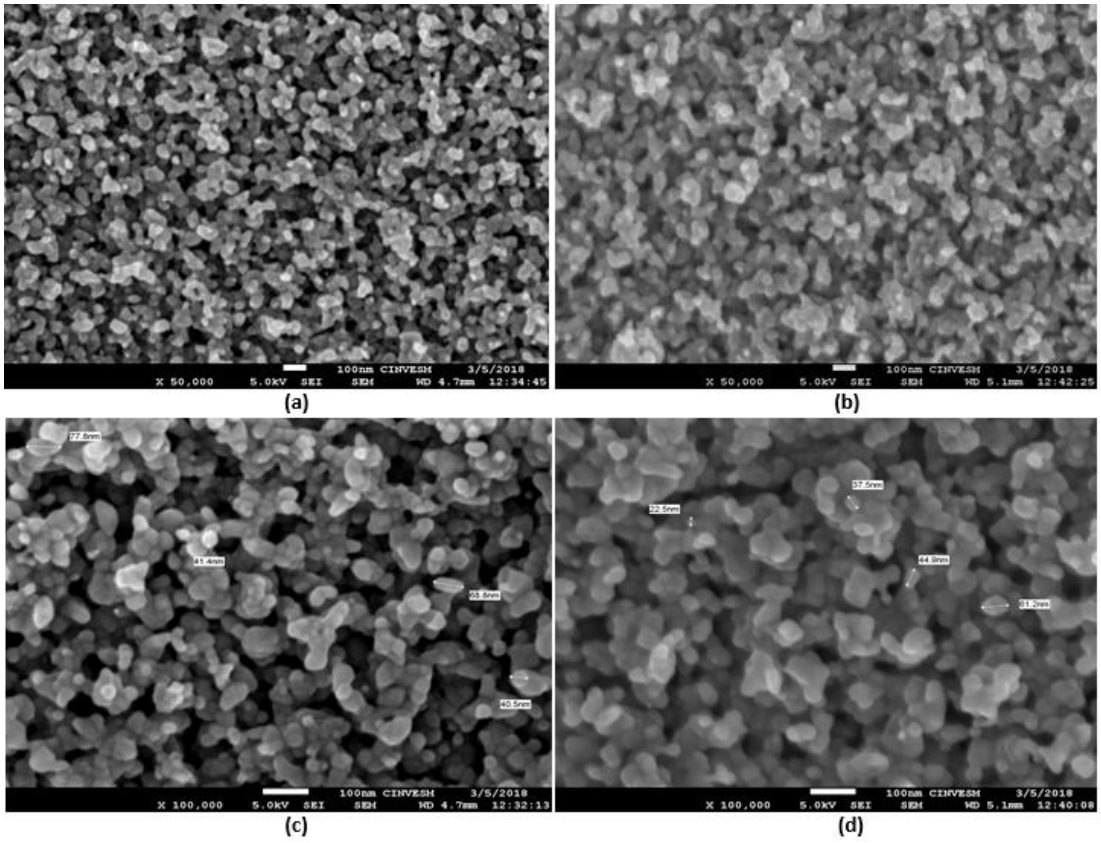

Figure 4. SEM images of ZnO thin films annealed at (a,c) 500 °C and (b,d) 600 °C with magnifications of 50,000X and 100,000X respectively.

EDS analysis was performed to evaluate the elemental composition of the films. The spectra obtained for the as-grown and annealed samples indicate the presence of only Zn and O elements, as shown in Figure 5. The Zn/O atomic ratios obtained from the EDS measurements are summarized in Table 1, showing a progressive increase in oxygen content with increasing annealing temperature, from 16.23% at the as-grown stage to 30.60% at 500 °C, consistent with the progressive thermal oxidation of metallic Zn into ZnO. A slight decrease in oxygen content is observed at 600 °C, which may result from the thermally induced evaporation of oxygen from the film surface at higher annealing temperatures. It is worth noting that the measured Zn/O ratios deviate from the expected 1:1 stoichiometry of ZnO, which can be attributed to the relatively low energy of the oxygen K-alpha X-ray line making it susceptible to absorption within the sample and leading to underestimation of the oxygen content, as well as systematic errors inherent to standardless EDS quantification for light elements. These factors are well-recognized limitations of EDS analysis, and the results should therefore be interpreted as qualitative confirmation of ZnO formation and progressive oxidation rather than precise stoichiometric quantification.

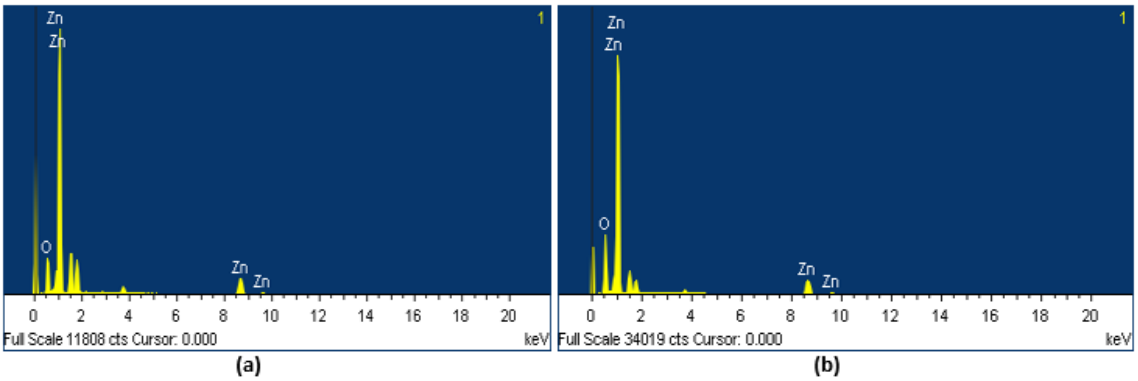

Figure 5. EDS spectra of ZnO thin films: (a) as-grown and (b) sample annealed at 600 °C.

The optical transmittance spectra of the as-grown and annealed Zn films are shown in Figure 6. The metallic Zn films that were annealed at temperatures up to 400 °C appear black and specular, resulting in negligible optical transmittance across the measured spectral range. In contrast, the films annealed at 500 °C and 600 °C become transparent to the naked eye and exhibit optical transmittance values close to 90% in the visible region. The increase in optical transmittance with annealing temperature indicates the progressive oxidation of metallic Zn and the formation of ZnO, which is consistent with the structural and compositional analyses discussed previously and with the Zn/O ratios reported in Table 1.

The optical band gap of the films annealed at 500 °C and 600 °C was estimated using the Tauc method, which relates the absorption coefficient near the absorption edge to the photon energy (Tauc et al., 1966). Assuming parabolic valence and conduction bands, the absorption coefficient of a semiconductor near the absorption edge can be expressed as:

$$(\alpha h\nu)^{\left(\frac{1}{n}\right)} = A\left(h\nu - E_g\right) \quad (1)$$

where A is a constant, E_g is the optical band gap, and n is a coefficient that depends on the nature of the electronic transition. For direct allowed transitions, such as those observed in ZnO, the value of n equals 1/2 (Özgür et al., 2005; Janotti & Van de Walle, 2009). The absorption coefficient α was calculated from the optical transmittance data using the relation (Manifacier et al., 1976):

$$\alpha = -\frac{1}{d}\ln\left(\frac{T}{1-R}\right) \quad (2)$$

where T is the optical transmittance, R is the reflectance, and d is the film thickness. Since the reflectance of ZnO thin films is relatively low in the visible and ultraviolet regions, this term can be neglected as a first approximation, allowing the absorption coefficient to be estimated directly from the transmittance data, simplifying equation (2) to:

$$\alpha = -\frac{\ln(T)}{d} \quad (3)$$

The calculated absorption coefficients and the corresponding Tauc plots are presented in Figure 6. The optical band gap values were determined by extrapolating the linear region of the absorption edge in the Tauc plots to the photon energy axis. The estimated optical band gap values of 3.22 eV and 3.25 eV for films annealed at 500 °C and 600 °C, respectively, are consistent with the typical band gap of ZnO and fall within the range of 3.20–3.37 eV widely reported for undoped polycrystalline ZnO thin films prepared by various deposition techniques, including RF magnetron sputtering and sol–gel methods (Özgür et al., 2005; Kołodziejczak-Radzimska & Jesionowski, 2014; Soylu & Coskun, 2018; Dave et al., 2016; Nabil et al., 2021). The slight increase in band gap from

3.22 to 3.25 eV with increasing annealing temperature is consistent with improved crystallinity and reduced defect density, which narrows the band tail states and shifts the absorption edge toward the bulk ZnO value. These results confirm that the thermal oxidation route employed in this work yields ZnO films with optical quality fully consistent with that achieved through more established and complex fabrication methods.

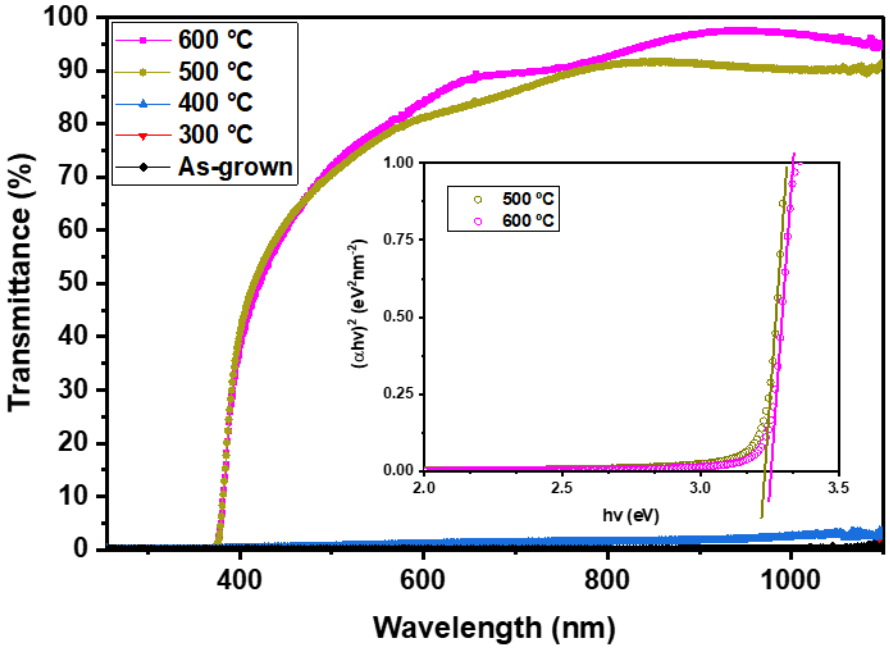

Figure 6. Optical transmittance spectra of the as-grown Zn thin film and ZnO thin films annealed at 300, 400, 500, and 600 °C. Inset: Tauc plots used to estimate the optical band gap of the films annealed at 500 °C and 600 °C.

The electrical properties of the films were evaluated using the Hall effect with the Van der Pauw method. The measurements were performed at room temperature for all samples after cooling from the annealing process. The obtained values of resistivity and carrier mobility as a function of annealing temperature are summarized in Table 1 and shown in Figure 7. The as-grown metallic Zn film exhibits a very low resistivity of approximately 7.91×10^{-5} Ω·cm, which is characteristic of metallic conduction. Due to the limitations of the Van der Pauw method for highly conductive metallic samples, reliable Hall mobility values could not be determined for this film.

After thermal annealing, the resistivity increases significantly as the metallic Zn layer is progressively oxidized to form ZnO, reaching values on the order of 10^{-2} to 10^{-1} Ω·cm for films annealed at 400 °C and above. This increase is consistent with the transition from metallic Zn to semiconducting ZnO and correlates with the increasing oxygen content observed in the EDS measurements also reported in Table 1. The obtained resistivity values fall within the range reported for undoped nanostructured ZnO thin films prepared by sputtering methods (Minami, 2005; Ellmer, 2012), confirming the successful formation of semiconducting ZnO through the thermal oxidation route.

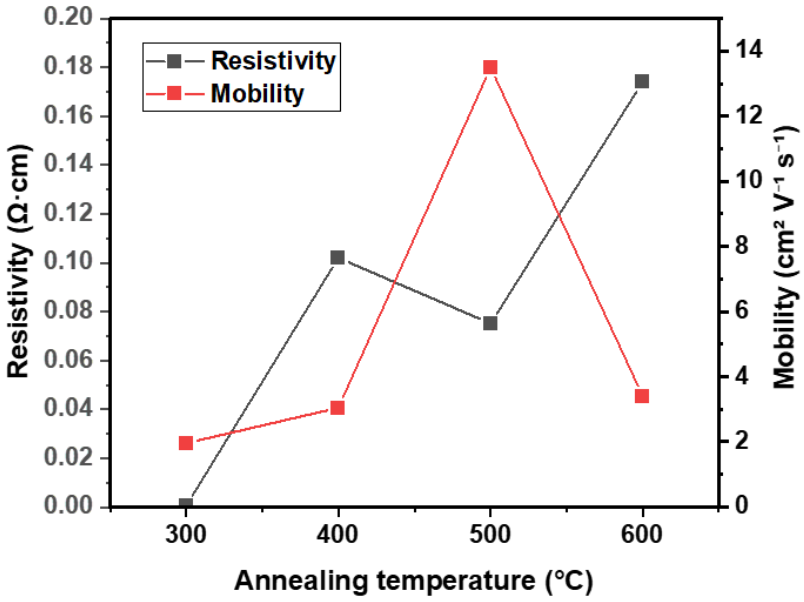

Figure 6. Electrical resistivity and carrier mobility of ZnO thin films as a function of annealing temperature measured by the Hall effect using the Van der Pauw method.

The carrier mobility shows a strong dependence on the annealing temperature, increasing significantly for the film annealed at 500 °C to a maximum value of approximately 13.5 $cm^2 \cdot V^{-1} \cdot s^{-1}$. This behavior is consistent with the improved crystallinity and grain growth observed at this temperature in the XRD and SEM analyses, where larger and more well-defined grains provide fewer grain boundary scattering sites for charge carriers, as evidenced by the SEM images in Figure 4. However, for the film annealed at 600 °C, carrier mobility decreases despite the continued improvement in crystalline order observed by XRD. This apparent discrepancy can be reconciled by distinguishing between two distinct classes of defects. The XRD analysis reflects a reduction in structural defects, such as lattice strain and dislocations, which manifests as narrower and more intense diffraction peaks with increasing annealing temperature. In contrast, the electrical behavior at 600 °C is governed by electrically active point defects, primarily oxygen vacancies and zinc interstitials, whose concentration may increase at higher annealing temperatures due to the thermally induced evaporation of zinc and oxygen atoms from the film surface (Janotti & Van de Walle, 2009; Li et al., 2020), consistent with the slight decrease in oxygen content observed in the EDS measurements at this temperature (Table 1). These point defects act as ionized impurity scattering centers, reducing carrier mobility independently of the degree of long-range crystalline order (Muthusamy et al., 2024). Thus, the reduction in structural defects and the increase in electrically active point defects are not contradictory but rather reflect the different physical mechanisms probed by XRD and Hall effect measurements, respectively. These results confirm that thermal oxidation of sputtered metallic Zn films is a simple and cost-effective approach for producing nanostructured ZnO thin films with electrical properties suitable for optoelectronic applications.

Table 1. Thickness, Zn/O atomic ratio (EDS), optical band gap, and electrical properties of the as-grown Zn film and samples annealed at different temperatures.

	As-grown	300 ºC	400 ºC	500 ºC	600 ºC
Thickness (nm)	316	400	632	464	656
Zn/O **ratio (%)**	$83.77/16.23$	$75.16/24.84$	$72.12/27.8$	$69.40/30.60$	$74.67/25.33$
Optical band gap (eV)	-	-	-	3.22	3.25
Resistivity (Ω·cm)	$7.91\text{x}10^{-5}$	$6.09\text{x}10^{-4}$	$1.02\text{x}10^{-1}$	$7.51\text{x}10^{-2}$	$1.74\text{x}10^{-1}$
Mobility ($cm^2 \cdot V^{-1} \cdot s^{-1}$)	-	1.96	3.05	13.5	3.4

Conclusions

ZnO thin films were successfully fabricated via the thermal oxidation of metallic Zn layers deposited on glass substrates by RF magnetron sputtering under non-reactive conditions, without the need for reactive gases during deposition. This approach avoids the target poisoning and process instability associated with reactive sputtering, offering a simpler and more reproducible route to nanostructured ZnO thin films for optoelectronic applications.

Structural characterization confirmed the formation of polycrystalline ZnO with a hexagonal wurtzite structure, with crystallinity progressively improving with annealing temperature. A key finding is the persistence of residual metallic Zn in films annealed at temperatures up to 400 °C, as evidenced by the (101) reflection of hexagonal close-packed Zn in the XRD patterns, while complete oxidation is achieved at 500 °C and above. This establishes 500 °C as a critical threshold temperature for the full conversion of sputtered Zn into crystalline ZnO under the conditions employed in this work.

Morphological analysis revealed nanostructured porous films with grain sizes ranging from approximately 14 to 74 nm, with annealing temperature serving as the primary control parameter for grain growth and structural reorganization. The combination of nanostructured porosity and progressive crystallization demonstrated here highlights the potential of this fabrication route for applications requiring high surface-to-volume ratios, such as gas sensing and photovoltaic electron transport layers.

Optical and electrical characterization showed that films annealed at 500 °C represent the optimal compromise between complete oxidation, high visible transmittance (~90%), and maximum carrier mobility (~13.5 $cm^2 \cdot V^{-1} \cdot s^{-1}$). The band gap values of 3.22–3.25 eV are consistent with high-quality ZnO, and the electrical properties fall within the range reported for undoped polycrystalline ZnO prepared by more complex deposition methods, demonstrating the competitiveness of this simple thermal oxidation route. The observed mobility decrease at 600 °C, attributed to an increase in electrically active point defects rather than structural disorder, provides important insight into the competing mechanisms governing carrier transport in thermally oxidized ZnO films.

Overall, this work demonstrates that annealing temperature alone is a powerful and sufficient parameter for tuning the structural, morphological, optical, and electrical properties of ZnO thin films obtained by thermal oxidation of RF-sputtered Zn. The simplicity, cost-effectiveness, and scalability of this fabrication route make it a promising candidate for the production of ZnO layers in a wide range of optoelectronic devices.

Acknowledgments

M.N. acknowledges support from SECIHTI through Estancias Posdoctorales por México program (CVU 785503).

References

Correa-Baena J.-P., Abate A., Saliba M., Tress W., Jesper Jacobsson T., Grätzel M., Hagfeldt A. (2017). The rapid evolution of highly efficient perovskite solar cells. Energy & Environmental Science, 10, 710–727.

Dave P. Y., Patel K. H., Chauhan K. V., Chawla A. K., Rawal S. K. (2016). Examination of zinc oxide films prepared by magnetron sputtering. Procedia Technology, 23, 328–335.

Ellmer K. (2001). Magnetron sputtering of transparent conductive zinc oxide: Relation between the sputtering parameters and the electronic properties. Journal of Physics D: Applied Physics, 34, 3097–3108.

Ellmer K. (2012). Past achievements and future challenges in the development of optically transparent electrodes. Nature Photonics, 6, 809–817.

Fortunato E., Ginley D., Hosono H., Paine D. C. (2012). Transparent conducting oxides for photovoltaics. MRS Bulletin, 37, 847–858.

Hoffmann R. C., Sanctis S., Liedke M. O., Butterling M., Wagner A., Njel C., Schneider J. J. (2021). Zinc oxide defect microstructure and surface chemistry derived from oxidation of metallic zinc: Thin-film transistor and sensor behavior of ZnO films and rods. *Chemistry – A European Journal*, 27, 5422–5431.

Janotti A., Van de Walle C. G. (2009). Fundamentals of zinc oxide as a semiconductor. Reports on Progress in Physics, 72, 126501.

Jeong S. H., Kim B. S., Lee B. T. (2003). Structural and optical properties of ZnO thin films deposited by RF magnetron sputtering. Applied Surface Science, 214, 191–196.

Kołodziejczak-Radzimska A., Jesionowski T. (2014). Zinc oxide—from synthesis to application: A review. Materials, 7, 2833–2881.

Law M., Greene L. E., Johnson J. C., Saykally R., Yang P. (2005). Nanowire dye-sensitized solar cells. Nature Materials, 4, 455–459.

Li W., Yin H., Mo H., Lai L., Fu S., Li L., Ye L., Xiong Y., Li H. (2020). Thermal evolution of point defects in indium doped ZnO transparent conducting films. *Thin Solid Films*, 713, 138350.

Li Z. W., Gao W., Reeves R. J. (2005). Zinc oxide films by thermal oxidation of zinc thin films. Surface and Coatings Technology, 198(1–3), 319–323.

Manifacier J. C., Gasiot J., Fillard J. P. (1976). A simple method for the determination of the optical constants n, k and the thickness of a weakly absorbing thin film. Journal of Physics E: Scientific Instruments, 9, 1002–1004.

Minami T. (2005). Transparent conducting oxide semiconductors for transparent electrodes. Semiconductor Science and Technology, 20, S35–S44.

Muthusamy S., Bharatan S., Sivaprakasam S., Mohanam R. (2024). Effect of deposition temperature on Zn interstitials and oxygen vacancies in RF-sputtered ZnO thin films and thin film-transistors. *Materials*, 17, 5153.

Nabil M., Perez-Quintana I. V., Acosta M., Mendez-Gamboa J. A., Castro-Rodriguez R. (2021). Morphological, structural, and optical bandgap characterization of extracted ZnO nanoparticles from commercial paste. Advances in Materials Science and Engineering, 2021, Article ID 9926544.

O'Regan B., Grätzel M. (1991). A low-cost, high-efficiency solar cell based on dye-sensitized colloidal TiO_2 films. Nature, 353, 737–740.

Özgür Ü., Alivov Y. I., Liu C., Teke A., Reshchikov M. A., Doğan S., Avrutin V., Cho S. J., Morkoç H. (2005). A comprehensive review of ZnO materials and devices. Journal of Applied Physics, 98(4), 041301.

Özgür Ü., Hofstetter D., Morkoç H. (2020). ZnO devices and applications: A review of current status and future prospects. Proceedings of the IEEE, 108, 1440–1471.

Raha S., Ahmaruzzaman M. (2022). ZnO nanostructured materials and their potential applications: progress, challenges and perspectives. Nanoscale Advances, 4(8), 1868–1925.

Raoufi D. (2013). Synthesis and microstructural properties of ZnO nanoparticles prepared by precipitation method. Renewable and Sustainable Energy Reviews, 26, 758–770.

Sánchez-Dena O., Hernández-López S., Camacho-López M. A., Acuña-Ávila P. E., Reyes-Esqueda J. A., Vigueras-Santiago E. (2022). ZnO films from thermal oxidation of Zn films: Effect of the thickness of the precursor films on the structural, morphological, and optical properties of the products. *Crystals*, 12, 528.

Soylu M., Coskun M. (2018). Controlling the properties of ZnO thin films by varying precursor concentration. Journal of Alloys and Compounds, 739, 1096–1103.

Tauc J., Grigorovici R., Vancu A. (1966). Optical properties and electronic structure of amorphous germanium. Physica Status Solidi, 15, 627–637.

White M. S., Olson D. C., Shaheen S. E., Kopidakis N., Ginley D. S. (2006). Inverted bulk heterojunction organic photovoltaic device using a solution-derived ZnO layer. Applied Physics Letters, 89, 143517.

Widyastuti E., Hsu J.-L., Lee Y.-C. (2022). Insight on photocatalytic and photoinduced antimicrobial properties of ZnO thin films deposited by HiPIMS through thermal oxidation. *Nanomaterials*, 12, 463.

Yang D., Yang R., Ren X., Zhu X., Yang Z., Li C., Liu S. (2016). Suppressing ZnO-induced decomposition in perovskite solar cells by chelating agent surface modification. ACS Applied Materials & Interfaces, 8, 31814–31820.